**Defense Threat Reduction Agency**
**8725 John J. Kingman Road, MS-6201**
**Fort Belvoir, VA 22060-6201**

**DTRA-TR-21-032 R1**

TECHNICAL REPORT

# A Time-Dependent Physiological Model of Innate and Adaptive Immune Responses Activated by Superficial Thermal Burns



October 2022

HDTRA1-14-D-0003

Prepared by:
Applied Research Associates, Inc.
801 N. Quincy Street
Suite 700
Arlington, VA 22203

# UNIT CONVERSION TABLE

**U.S. customary units to and from international units of measurement***

| U.S. Customary Units | Multiply by → / ← Divide by† | | International Units |
|---|---|---|---|
| **Length/Area/Volume** | | | |
| inch (in) | 2.54 | $\times 10^{-2}$ | meter (m) |
| foot (ft) | 3.048 | $\times 10^{-1}$ | meter (m) |
| yard (yd) | 9.144 | $\times 10^{-1}$ | meter (m) |
| mile (mi, international) | 1.609 344 | $\times 10^{3}$ | meter (m) |
| mile (nmi, nautical, U.S.) | 1.852 | $\times 10^{3}$ | meter (m) |
| barn (b) | 1 | $\times 10^{-28}$ | square meter ($m^2$) |
| gallon (gal, U.S. liquid) | 3.785 412 | $\times 10^{-3}$ | cubic meter ($m^3$) |
| cubic foot ($ft^3$) | 2.831 685 | $\times 10^{-2}$ | cubic meter ($m^3$) |
| **Mass/Density** | | | |
| pound (lb) | 4.535 924 | $\times 10^{-1}$ | kilogram (kg) |
| atomic mass unit (AMU) | 1.660 539 | $\times 10^{-27}$ | kilogram (kg) |
| pound-mass per cubic foot ($lb\ ft^{-3}$) | 1.601 846 | $\times 10^{1}$ | kilogram per cubic meter ($kg\ m^{-3}$) |
| Pound-force (lbf avoirdupois) | 4.448 222 | | Newton (N) |
| **Energy/Work/Power** | | | |
| electron volt (eV) | 1.602 177 | $\times 10^{-19}$ | joule (J) |
| erg | 1 | $\times 10^{-7}$ | joule (J) |
| kiloton (kT) (TNT equivalent) | 4.184 | $\times 10^{12}$ | joule (J) |
| British thermal unit (Btu) (thermochemical) | 1.054 350 | $\times 10^{3}$ | joule (J) |
| foot-pound-force (ft lbf) | 1.355 818 | | joule (J) |
| calorie (cal) (thermochemical) | 4.184 | | joule (J) |
| **Pressure** | | | |
| atmosphere (atm) | 1.013 250 | $\times 10^{5}$ | pascal (Pa) |
| pound force per square inch (psi) | 6.984 757 | $\times 10^{3}$ | pascal (Pa) |
| **Temperature** | | | |
| degree Fahrenheit (°F) | [T(°F) − 32]/1.8 | | degree Celsius (°C) |
| degree Fahrenheit (°F) | [T(°F) + 459.67]/1.8 | | kelvin (K) |
| **Radiation** | | | |
| activity of radionuclides [curie (Ci)] | 3.7 | $\times 10^{10}$ | per second ($s^{-1}$‡) |
| air exposure [roentgen (R)] | 2.579 760 | $\times 10^{-4}$ | coulomb per kilogram ($C\ kg^{-1}$) |
| absorbed dose (rad) | 1 | $\times 10^{-2}$ | joule per kilogram ($J\ kg^{-1}$§) |
| equivalent and effective dose (rem) | 1 | $\times 10^{-2}$ | joule per kilogram ($J\ kg^{-1}$**) |

*Specific details regarding the implementation of SI units may be viewed at http://www.bipm.org/en/si/.

†Multiply the U.S. customary unit by the factor to get the international unit. Divide the international unit by the factor to get the U.S. customary unit.

‡The special name for the SI unit of the activity of a radionuclide is the becquerel (Bq). ($1\ Bq = 1\ s^{-1}$).

§The special name for the SI unit of absorbed dose is the gray (Gy). ($1\ Gy = 1\ J\ kg^{-1}$).

**The special name for the SI unit of equivalent and effective dose is the sievert (Sv). ($1\ Sv = 1\ J\ kg^{-1}$).

# REPORT DOCUMENTATION PAGE

**PLEASE DO NOT RETURN YOUR FORM TO THE ABOVE ORGANIZATION.**

| 1. REPORT DATE | 2. REPORT TYPE | 3. DATES COVERED | |
|---|---|---|---|
| | | START DATE | END DATE |
| 10-19-2022 | Technical Report | | |

**4. TITLE AND SUBTITLE**

A Time-Dependent Physiological Model of Innate and Adaptive Immune Responses Activated by Superficial Thermal Burns

| 5a. CONTRACT NUMBER | 5b. GRANT NUMBER | 5c. PROGRAM ELEMENT NUMBER |
|---|---|---|
| HDTRA1-14-D-0003 | | |
| **5d. PROJECT NUMBER** | **5e. TASK NUMBER** | **5f. WORK UNIT NUMBER** |
| | | |


**6. AUTHOR(S)**

Rachel Jennings, PhD, Amy Creel, Angela Reynolds, PhD,

**7. PERFORMING ORGANIZATION NAME(S) AND ADDRESS(ES)**

Applied Research Associates, Inc.
801 N. Quincy Street, Suite 700
Arlington, VA 22203


**8. PERFORMING ORGANIZATION REPORT NUMBER**

| 9. SPONSORING/MONITORING AGENCY NAME(S) AND ADDRESS(ES) | 10. SPONSOR/MONITOR'S ACRONYM(S) | 11. SPONSOR/MONITOR'S REPORT NUMBER(S) |
|---|---|---|
| Defense Threat Reduction Agency - Nuclear Technologies Department, Attn: Dr. Blake<br>8725 John J. Kingman Road, Mail Stop 6201<br>Fort Belvoir, VA 22060-6201 | DTRA-RD-NTS | DTRA-TR-21-032 R1 |

**12. DISTRIBUTION/AVAILABILITY STATEMENT**

DISTRIBUTION A. Approved for public release: distribution is unlimited.

**13. SUPPLEMENTARY NOTES**


**14. ABSTRACT**

The physiological mechanisms activated in response to superficial thermal burns follow the normal progression of wound healing. In this work, a time-dependent physiological model is formulated to capture both hematopoietic and immunologic events across the bone marrow, lymphatic tissues, blood vessels and local wound site. The model is then reduced to examine only local inflammatory dynamics at the burn site. Numerical simulations are provided conducted to assess the model's capability to reproduce known and feasible biological behavior.



**15. SUBJECT TERMS**

Thermal Burn, Wound Healing, Inflammation, Modeling, ODEs


| 16. SECURITY CLASSIFICATION OF: | | | 17. LIMITATION OF ABSTRACT | 18. NUMBER OF PAGES |
|---|---|---|---|---|
| a. REPORT | b. ABSTRACT | C. THIS PAGE | | |
| U | U | U | U | 35 |

| 19a. NAME OF RESPONSIBLE PERSON | 19b. PHONE NUMBER *(Include area code)* |
|---|---|
| Paul K. Blake, PhD, GS-15 | 571.616.6117 |



PREVIOUS EDITION IS OBSOLETE.

**STANDARD FORM 298 (REV. 5/2020)**
*Prescribed by ANSI Std. Z39.18*

This page intentionally left blank.

# Table of Contents

# List of Figures

# List of Tables

# Revision Notes

## Rev 1

This revision includes an expansion of the type of thermal injury considered from first-degree (superficial thickness) only to superficial thermal burns (superficial thickness and minor superficial partial thickness). The Title was modified to reflect this change. Further, all mentions of "first-degree thermal burns" were replaced with "superficial thermal burns" throughout the report to reflect this change.

Additionally, this revision includes modifications to the mathematical model equations. These modifications include expanding the model to account for debris at the wound site in addition to damaged tissue (e.g., Equation 14 is new); including a damaged tissue-dependent multiplier term for fibroblast activation and proliferation (see Equation 23); revising the macrophage phenotype transition rate from M1 to M2 to depend on the apoptosis rate of neutrophils by M1 macrophage (see Equations 18 and 19)s; and changing other inhibitory terms to better reflect the biology. Table 1, Figure 1, Section 4.2, Sections 4.3.4-4.3.7, Equations 35-42, and Table 3 were revised to reflect these changes. The notation for the auxiliary equations was also simplified (see Equations 29-33). The numerical simulations presented in Section 6 were streamlined to include the important features of the model. Subsections *Healing in the Absence of Neutrophils* and *Impact of Acute Immunosuppression* were removed. *"Normal" Healing Dynamics* was merged with *Sensitivity to Initial Damage* to cover both types of superficial burns considered (superficial thickness and superficial partial thickness burn), allowing for the types of injuries considered to be expanded to superficial thermal burns instead of only first-degree. Table 2 was updated to reflect this change. A new subsection (now 6.2, *Healing Without Removal of Debris*) was added to study the impact of debris removal failure on the normal healing process.

The Purpose section was also removed as part of this revision

# Acknowledgements

We gratefully acknowledge Dr. Paul Blake, Ms. Minoo Rouhanian, and DTRA's Nuclear Technologies Survivability Division for programmatic support. We would also like to acknowledge the contributions of Dr. David Schauer, COL Mohammad Naeem, Col Pamela Ward-Demo, MAJ Omololu Makinde, LT Elih Velazquez, and LTC Mitchell Woodberry (SRD) of the Armed Forces Radiobiology Research Institute for their support and valuable feedback that helped shape this technical report. This work was performed under DTRA contract HDTRA1-14-D-0003.

# Executive Summary

The physiological mechanisms activated in response to superficial thermal burns follow the normal progression of wound healing, which is comprised of four distinct yet overlapping phases (hemostasis, inflammation, proliferation, and remodeling). In this work, a time-dependent physiological model governed by 23 ordinary differential equations is formulated to capture both hematopoietic and immunologic events across the bone marrow, lymphatic tissues, blood vessels and local wound site. As superficial thermal injuries do not disrupt hematopoietic homeostasis, the model reduces to a subsystem describing innate and adaptive immune dynamics as well as early fibroblast activity at the injury location. Numerical simulations are then conducted to assess the model's capability to reproduce known and feasible biological behavior following superficial thermal burns. The model will later serve as a foundational structure for the construction of physiologically driven models that not only adopt systems-level mechanistic frameworks but also leverage legacy models developed by the Defense Threat Reduction Agency to predict casualty distributions after a nuclear detonation event (i.e., those that have been implemented into the Health Effects from Nuclear and Radiological Environments tool such as the granulopoiesis and lymphopoiesis models). Specifically, once the model has been augmented to include a sufficient range of thermal burn injury and the effects of ionizing radiation exposure, we aim to develop a method to transform the time-series output of the model to predict mortality and morbidity outcomes for combined injury resulting from nuclear detonation environments.

# Section 1. Introduction

As part of its mission to safeguard against weapons of mass destruction, the Defense Threat Reduction Agency (DTRA) developed Health Effects from Nuclear and Radiological Environments (HENRE), a modeling program consisting of a suite of advanced empirical and mechanistic-based mathematical models designed to estimate the health effects for individuals exposed to nuclear detonation (NUDET) environments. Following a NUDET event, historical evidence suggests that well over half of the resulting casualties will have some level of radiation exposure in conjunction with another trauma (Oughterson et al. 1951; Dicarlo et al. 2020). Thus, it is reasonable that the number of casualties experiencing combined injury[1] will be even greater. Understanding the collective effects of combined injury, including the complex pathophysiology due to potential synergy, is fundamental for gauging injury severity and outcome. Therefore, it is critical to assess the severity of these coinciding injuries in order to identify the potential health complications that can hinder performance for military personnel, strain medical resources, and lead to morbidity and mortality for individuals exposed to the NUDET environments. Although HENRE is comprised of a dynamic library of models, those pertaining to combined injury as of the date of this publication are limited and are strictly empirically based; that is, few utilize output from a time-dependent physiological model (TDPM) describing pathological effects following an insult. Modeling the aggregated effects of combined injury poses several challenges, such as varying insult exposures, wide-ranging injury severity, multiple sites of injury, inconsistent time-to-onset of symptoms across insults, gender, and age variability, and limited available datasets.

[1] Combined injury, more generally, refers to the injury resulting from two or more insults impacting the body simultaneously or near so.

# Section 2. Purpose

The purpose of this technical report (TR) is to present a TDPM for the local healing of superficial thermal burn wounds that will serve as a foundational structure for the development of physiologically driven models of combined injury. The TDPM characterizes local inflammation with innate and adaptive immune responses, as well as initial fibroblast activity after tissue injury. Numerical simulations with the TDPM will demonstrate the ability of the model to produce biologically sound results and to discuss model dynamics in the case of normal wound healing. Some parameters of the TDPM will then be perturbed from their baseline values, which are taken to be a specific set in which the wound heals normally, to display changes in model behavior and the progression of wound healing over time in various scenarios. This TR will not discuss in detail the parameter estimation process or the process of wound healing for other insult environments and for higher intensity thermal burns, as these will be discussed in future work.

# Section 3. Wound Healing Under Fire

Thermal burns stem from absorption of thermal fluence by exposed skin, resulting in cell and tissue damage at varying depths; those that penetrate deeper levels of the skin are considered more severe (Evers et al. 2010). The physiological processes initiated by thermal burns- regardless of severity- follows the four phases of wound healing: hemostasis, inflammation, proliferation, and remodeling (Diegelmann and Evans 2004; Strudwick and Cowin 2018; Abazari et al. 2020). However, the modeling effort described therein focuses on superficial thermal burns, which is defined as superficial thickness (first-degree) and minor[2] partial thickness (second-degree) injuries in which timely healing occurs without scarring and intervention, and there is no or negligible risk of secondary infection (Evers et al. 2010; Wang 2014; Reeves 2018; Abazari et al. 2020; Jeschke et al. 2020).

To build a mathematical model of the wound healing cascade following superficial thermal burn injury, we must first understand the "simplest" wound where healing always occurs. This understanding will provide us with a foundation of "healthy" dynamics that can be expanded to incorporate different pathological profiles. This model will serve as a base (or "healthy") case. Below we provide a brief characterization of wound healing in terms of its four phases and highlight healing dynamics distinct to superficial thermal burns.

## 3.1 Hemostasis

Hemostasis, in general, begins immediately following tissue injury to stop bleeding while not impeding the circulation of blood flow outside of the local tissue damage (Gale 2011). Towards the end of this phase, various signaling molecules[3] released by platelets recruit neutrophils and macrophages to the wound site (Goldberg and Diegelmann 2010). Although bleeding does not result from thermal burn (Abazari et al. 2020), and therefore there is no need for vasoconstriction (constriction of blood cells, which decreases blood flow) or vasodilation (the dilation of blood cells, which increases blood flow), this phase still occurs in these wounds and is characterized by heightened capillary permeability (Tiwari 2012).

## 3.2 Inflammation

The inflammatory phase follows hemostasis and prepares the wound site for tissue repair. Symptoms often associated with inflammation include redness, pain, heat, and swelling (Goldberg and Diegelmann 2010). Both the innate (neutrophils and macrophages) and the adaptive (T lymphocytes) immune responses play key roles during this phase (Barton 2008). Circulating neutrophils are recruited by signaling molecules and infiltrate the wound site through the extracellular matrix in a manner that aims to avoid causing further tissue damage (Buganza Tepole and Kuhl 2013), (Kotwal and Chien 2017), (Van Linthout et al. 2014). Once they arrive at the wound site, neutrophils phagocytize any debris[4] resulting from injury (Ellis et al. 2018; Wilkinson and Hardman 2020). Neutrophil recruitment continues anywhere from one to several days, using signaling molecules to amplify the pro-inflammatory response (Buganza Tepole and Kuhl 2013).

Arriving shortly after neutrophils, activated macrophages are derived from fixed-tissue and circulating monocytes, and they exhibit phagocytic behavior similar to that of neutrophils, allowing them to clear tissue debris in the absence of neutrophils as well as ingest bacteria and debris-laden neutrophils that have moved into an apoptotic state (Goldberg and Diegelmann 2010). Macrophages produce signaling molecules that recruit a range of immune cells to the wound site. Upon migration to the injury site, monocytes differentiate

[2] Here, minor refers to less than 20% total body surface area (Jeschke et al. 2020).

[3] Signaling molecules is used to indicate growth factors, cytokines, chemokines, and other proteins/enzymes.

[4] Here, debris refers to any bacteria, damaged extracellular components, and foreign materials present in the wound site following injury.

into two phenotypes: pro- inflammatory (M1) and anti-inflammatory (M2). M1 macrophages are responsible for cleaning debris from the wound site (Krzyszczyk et al. 2018) and exhibit phagocytic behavior (Hesketh et al. 2017); that is, the M1 phenotype demonstrates neutrophil-like functions. In contrast, M2 macrophages promote tissue repair as well as play a key role in suppressing pro-inflammation (Hesketh et al. 2017; Krzyszczyk et al. 2018). While macrophage function exists on a spectrum with M1 and M2 acting as end points, increasing evidence suggests polarization of macrophage function towards one of these phenotypes impedes the healing process (Ferrante and Leibovich 2012; Pinto et al. 2016; Krzyszczyk et al. 2018; Meziani et al. 2018; Čoma et al. 2021). T lymphocytes, which include TH1 cells, TH2 cells, TH17 cells, γδ-T cells and Tregs, have been reported to enter the wound site at varying points during the inflammation phase, but typically arrive shortly after macrophages (Abazari et al. 2020). Like macrophages, T lymphocytes exhibit pro-inflammatory and anti-inflammatory phenotypes (Murphy and Weaver 2017), (Romagnani 1999), and while they do not exhibit phagocytic behavior, they produce a range of signaling molecules that drive and amplify macrophage dynamics (Paulnock 1992), (Romagnani 1999) (and vice versa (Arnold et al. 2016), (Mills and Ley 2014)), advancing the transition of the anti-inflammatory profile required to resolve inflammation.

In response to thermal burns, inflammation typically manifests within a few hours and can last up to a couple days or longer, depending on the extent of the tissue damage (Sanghvi 2020). Neutrophil, macrophage and T lymphocyte migration to the wound site is delayed due to damaged blood vessels, resulting in an immunosuppressive state (Abazari et al. 2020), (Entezami and Mosavi 2017). When normal wound healing is impaired by sustained, pathological inflammation, there is an increase of downstream adverse outcomes, such as infections, sepsis, and multi-organ dysfunction (Church et al. 2006), (Baue et al. 1998). However, this risk is proportional to the depth of the thermal burn (Strudwick and Cowin 2018), making these complications rare following superficial burns.

## 3.3 Proliferation

During inflammation, proliferation begins when the signaling molecules released by neutrophils and macrophages activate fibroblasts and epithelial cells (Goldberg and Diegelmann 2010). This phase of wound healing aims to restore the original structure and function of the damaged tissue (Schultz et al. 2011) and is heavily reliant on fibroblast proliferation and migration to the local wound site (Goldberg and Diegelmann 2010); in fact, fibroblasts are critical to controlling tissue damage (Kotwal and Chien 2017), (Van Linthout et al. 2014). The proliferation phase associated with superficial thermal burns parallels that observed during normal wound healing (Strudwick and Cowin 2018).

## 3.4 Remodeling

Remodeling, the final phase, begins once granulation tissue has formed during proliferation (Orsted et al. 2016), and ends with the maturation of granulation tissue into a scar with tissue strength that resembles at most 80% of its pre-injury tensile strength (Goldberg and Diegelmann 2010). Hyperpigmentation can occur in superficial burns due to an overactive response of melanocytes to the burn injury (Tiwari 2012).

# Section 4. A Time-Dependent Physiological Model

Given its relevance to combined injury, which is the broader goal of this work, we first present a time-dependent physiological model (TDPM) of wound healing incorporating 1) innate and adaptive immune responses at local and systemic levels and 2) initial local fibroblast activity associated with the proliferation phase. To capture dynamics following a superficial burn wound, the TDPM is then reduced in scope in Section 5 using several simplifying and biologically supported assumptions appropriate for such burns. In both models, we assume the thermal insult level is sufficiently low to not warrant consideration of the introduction of pathogens into the local wound site.

## 4.1 Model Compartments and Variables

To capture the critical physiological responses characterizing inflammation and early proliferation following thermal burn, a model consisting of 23 ordinary differential equations (ODEs). Table 1 lists the symbols and corresponding descriptions of the state (or dynamic) variables[5] included in the TPDM. Figure 1 provides a schematic of the state variables and their relationships across four different compartments: 1) the bone marrow; 2) lymphatic tissues (i.e., lymph nodes, thymus, and spleen); 3) blood vessels (systemic dynamics); and 4) the (local) thermal burn wound. State variables are represented using circles and squares. The solid black lines indicate how the different cellular states flow within and between the four different compartments. Solid lines that feedback into the state variable itself indicate proliferation. Cellular interactions initiated by first degree burns are captured by dotted lines and remain locally concentrated. Blue and white colors are used to distinguish between up-regulatory (i.e., increasing in response to the cells themselves or the cells' signaling molecules) and destructive/inhibitory relationships, respectively.

[5] State (or dynamic) variables refer to those quantities whose temporal evolution will eventually be described by a system of ordinary differential equations (ODEs), reflecting that their levels change with time.

**Table 1. TDPM State Variable Symbols and Definitions by Compartment.**

| SYMBOL | DESCRIPTION |
|---|---|
| $\boldsymbol{t}$ | Time (in hours) |
| *Bone Marrow* | |
| $\boldsymbol{G^{*}_{bm}}$ | Granulocyte mitogenic progenitors in the bone marrow |
| $\boldsymbol{G^{**}_{bm}}$ | Granulocyte non-mitogenic progenitors in the bone marrow |
| $\boldsymbol{M^{*}_{bm}}$ | Monocyte mitogenic progenitors in the bone marrow |
| $\boldsymbol{M^{**}_{bm}}$ | Monocyte non-mitogenic progenitors in the bone marrow |
| $\boldsymbol{L^{*}_{bm}}$ | T lymphocyte mitogenic progenitors |
| *Lymphatic Tissues* | |
| $\boldsymbol{L^{**}_{lt}}$ | T lymphocyte non-mitogenic progenitors in the lymphatic tissues |
| $\boldsymbol{\bar{L}_{lt}}$ | Naïve, mature T lymphocytes in the lymphatic tissues |
| $\boldsymbol{L_{lt}}$ | Activated (effector) T lymphocytes in the lymphatic tissues |
| *Blood Vessels* | |
| $\boldsymbol{\bar{L}_{bv}}$ | Naïve, mature T lymphocytes in circulation |
| $\boldsymbol{L_{bv}}$ | Newly activated circulating T lymphocytes migrating to the site(s) of injury |
| $\boldsymbol{\bar{N}_{bv}}$ | Circulating neutrophils |
| $\boldsymbol{\bar{M}_{bv}}$ | Circulating monocytes |
| *Local Thermal Burn* | |
| $\boldsymbol{\mathrm{Dam}_{tb}}$ | Damaged tissue (unitless) |
| $\boldsymbol{Deb_{tb}}$ | Debris (unitless) |
| $\boldsymbol{\bar{N}_{tb}}$ | Neutrophils recruited to the burn site |
| $\boldsymbol{N_{tb}}$ | Activated neutrophils at the burn site |
| $\boldsymbol{\bar{M}_{tb}}$ | Resting monocytes and tissue-resident macrophages recruited to the burn site |
| $\boldsymbol{M1_{tb}}$ | Classically activated macrophages (M1) at the burn site |
| $\boldsymbol{M2_{tb}}$ | Alternatively activated macrophages (M2) at the burn site |
| $\boldsymbol{F_{tb}}$ | Fibroblasts at the burn site |
| $\boldsymbol{L_{tb}}$ | Activated (effector) T lymphocytes recruited to the burn site |
| $\boldsymbol{L1_{tb}}$ | Pro-inflammatory T lymphocytes, including $\gamma\delta$-T cells, TH1 cells, and TH17 cells, at the burn site |
| $\boldsymbol{L2_{tb}}$ | Anti-inflammatory T lymphocytes, which includes TH2 cells, and regulatory T cells, at the burn site |

An ODE was constructed for each state variable based on known physiological behaviors and interactions supported by peer-reviewed literature. Let $G/N$, $M$, and $L$ denote granulocyte/neutrophil, monocyte/macrophage, and T lymphocyte populations, respectively, with subscripts ($bm, lt, bv,$ and $tb$) indicating the compartment. For immature hematopoietic cells, single and double asterisks delineate between mitogenic and post-mitogenic progenitors. Similarly, immune response variables with the bar notation represent resting (or inactivated) cells, ergo capital letters with no additional markings denote activated cell populations. Certain state variables are unique to the thermal burn location; these include distinct macrophage ($M1_{tb}/M2_{tb}$) and T lymphocyte ($L1_{tb}/L2_{tb}$) phenotypes, activated tissue fibroblasts ($F_{tb}$), and degree of damaged tissue ($D_{tb}$). Modeling the different interactions between these state variables requires that we express their complex interactions mathematically, which involves a delicate balance between the biology and mathematics. To do such, it is assumed that each state variable not only represents the specific cell type but also its related signaling process. As a result, currently, no biological units of

measurement are explicitly assigned to each state variable. This is something that will be addressed in future work during the parameterization process.

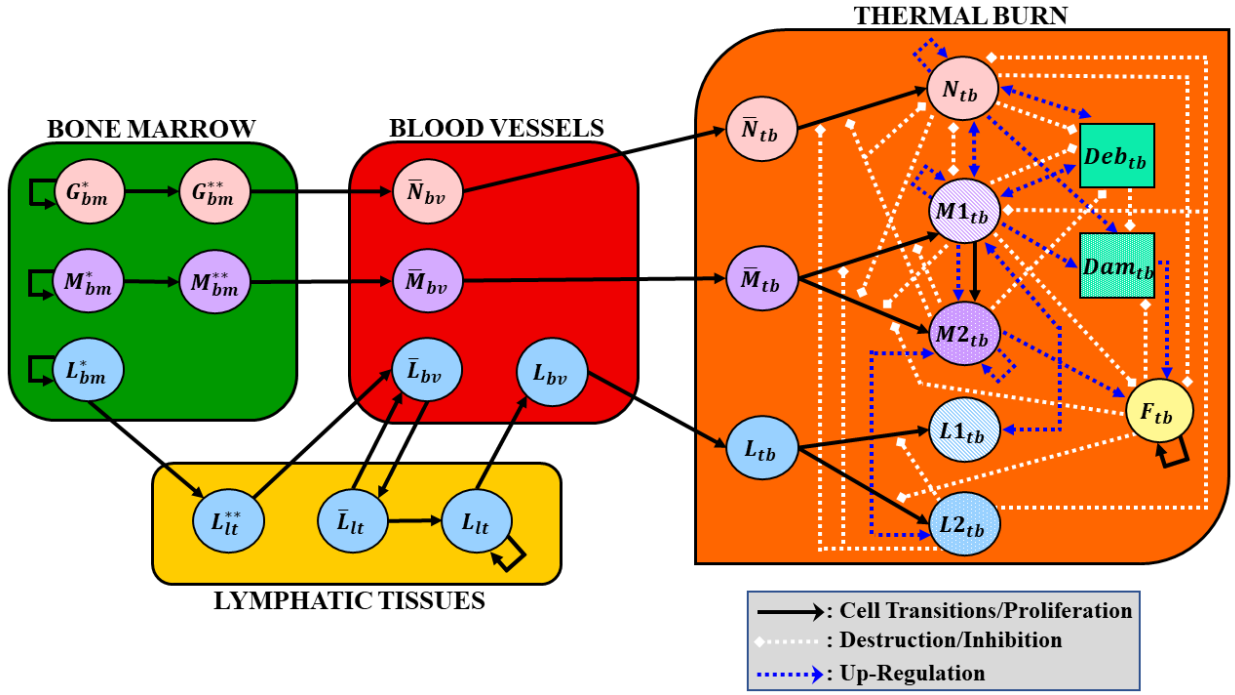


**Figure 1. Schematic diagram of the four TDPM compartments, the component state variables in each, and their relationships.**

## 4.2 Model Equations

The TDPM aims to link hematopoiesis to local inflammation and early fibroblast activity of wound healing following thermal burn. It is assumed the model is governed by the following system of equations (listed by compartment):

*BONE MARROW*

$$\frac{dG^*_{bm}}{dt} = [B_n(G^*_{bm},\ G^{**}_{bm}, \bar{N}_{bv}, \bar{N}_{tb}) - \eta_{bmbm}]G^*_{bm}, \tag{1}$$

$$\frac{dG^{**}_{bm}}{dt} = \eta_{bmbm}G^*_{bm}\ - \Delta_n(\bar{N}_{bv})G^{**}_{bm}, \tag{2}$$

$$\frac{dM^*_{bm}}{dt} = [B_m(M^*_{bm},\ M^{**}_{bm}, \bar{M}_{bv}, \bar{M}_{tb}) - \mu_{bmbm}]M^*_{bm}, \tag{3}$$

$$\frac{dM^{**}_{bm}}{dt} = \mu_{bmbm}M^*_{bm}\ - \Delta_m(\bar{M}_{bv})M^{**}_{bm}, \tag{4}$$

$$\frac{dL^*_{bm}}{dt} = [B_l(L^*_{bm}, L^{**}_{lt}, \bar{L}_{bv}) - \lambda_{bmlt}]L^*_{bm}, \tag{5}$$

*LYMPHATIC TISSUES*

$$\frac{dL_{lt}^{**}}{dt} = \lambda_{bmlt} L_{bm}^{*} - \lambda_{ltbv}^{*} L_{lt}^{**}, \tag{6}$$

$$\frac{d\bar{L}_{lt}}{dt} = \bar{\lambda}_{bvlt} \bar{L}_{bv} - \bar{\lambda}_{ltbv} \bar{L}_{lt} - \bar{\bar{\lambda}}_{ltlt} \bar{L}_{lt} - \bar{d}_l \bar{L}_{lt}, \tag{7}$$

$$\frac{dL_{lt}}{dt} = \bar{\bar{\lambda}}_{ltlt} \bar{L}_{lt} - \lambda_{ltbv} L_{lt} + \rho_l L_{lt}, \tag{8}$$

*BLOOD VESSELS*

$$\frac{d\bar{L}_{bv}}{dt} = \lambda_{ltbv}^{*} L_{lt}^{**} - \bar{\lambda}_{bvlt} \bar{L}_{bv} + \bar{\lambda}_{ltbv} \bar{L}_{lt} - \bar{d}_l \bar{L}_{bv}, \tag{9}$$

$$\frac{dL_{bv}}{dt} = \lambda_{ltbv} L_{lt} - \lambda_{bvtb} L_{bv} - d_l L_{bv}, \tag{10}$$

$$\frac{d\bar{N}_{bv}}{dt} = \Delta_n(\bar{N}_{bv}) G_{bm}^{**} - \bar{\eta}_{bvtb} \bar{N}_{bv} - \bar{d}_n \bar{N}_{bv}, \tag{11}$$

$$\frac{d\bar{M}_{bv}}{dt} = \Delta_m(\bar{M}_{bv}) M_{bm}^{**} - \bar{\mu}_{bvtb} \bar{M}_{bv} - \bar{d}_m \bar{M}_{bv}, \tag{12}$$

*LOCAL THERMAL BURN*

$$\begin{aligned}\frac{dDam_{tb}}{dt} = {} & k_{dn}\Omega_H(\Omega_i(N_{tb}; L2_{tb}, L2_2^{\infty}), 6, N_H) + \sigma_{m1} k_{dn}\Omega_H(\Omega_i(M1_{tb}; L2_{tb}, L2_2^{\infty}), 6, M1_H) \\ & - \rho_{dam}\Omega_i(Dam_{tb}; Deb_{tb}, Deb_{dam}^{\infty}) - k_{df} F_{tb}\Omega_i(Dam_{tb}; Deb_{tb}, Deb_{dam}^{\infty})\end{aligned} \tag{13}$$

$$\begin{aligned}\frac{dDeb_{tb}}{dt} = {} & k_{dn}\Omega_H(\Omega_i(N_{tb}; L2_{tb}, L2_2^{\infty}), 6, N_H) + \sigma_{m1} k_{dn}\Omega_H(\Omega_i(M1_{tb}; L2_{tb}, L2_2^{\infty}), 6, M1_H) \\ & - k_{dnp} N_{tb}\Omega_H(Deb_{tb}, 1, Deb_H) - k_{dm1p}\Omega_i(M1_{tb}; N_{tb}, N_1^{\infty})\Omega_H(Deb_{tb}, 1, Deb_H) \\ & - k_{dm2p}\Omega_i(M2_{tb}; N_{tb}, N_1^{\infty})\Omega_H(Deb_{tb}, 1, Deb_H) - d_{deb} Deb_{tb}\end{aligned} \tag{14}$$

$$\frac{d\bar{N}_{tb}}{dt} = \bar{\eta}_{bvtb} \bar{N}_{bv} - R_n \bar{N}_{tb} - d_{nr} \bar{N}_{tb} \tag{15}$$

$$\frac{dN_{tb}}{dt} = R_n \bar{N}_{tb} - k_{nm1p} N_{tb}\Omega_i(M1_{tb}; N_{tb}, N_1^{\infty}) - k_{nm2p} N_{tb}\Omega_i(M2_{tb}; N_{tb}, N_1^{\infty}) - d_n N_{tb} \tag{16}$$

$$\frac{d\bar{M}_{tb}}{dt} = \bar{\mu}_{bvtb} \bar{M}_{bv} - R_{m1} \bar{M}_{tb} - R_{m2} \bar{M}_{tb} - d_{mr} \bar{M}_{tb} \tag{17}$$

$$\frac{dM1_{tb}}{dt} = R_{m1} \bar{M}_{tb} - \theta_{m1m2} [k_{nm1p} N_{tb}\Omega_i(M1_{tb}; N_{tb}, N_1^{\infty})] + \theta_{m2m1} M2_{tb} - d_{m1} M1_{tb} \tag{18}$$

$$\frac{dM2_{tb}}{dt} = R_{m2} \bar{M}_{tb} + \theta_{m1m2} [k_{nm1p} N_{tb}\Omega_i(M1_{tb}; N_{tb}, N_1^{\infty})] - \theta_{m2m1} M2_{tb} - d_{m2} M2_{tb} \tag{19}$$

$$\frac{dL_{tb}}{dt} = \lambda_{bvtb} L_{bv} - k_{l1} L_{tb}\Omega_i(M1_{tb}; L2_{tb}, L2_1^{\infty}) - k_{l2} L_{tb}\Omega_i(M2_{tb}; F_{tb}, F^{\infty}) - d_{lr} L_{tb} \tag{20}$$

$$\frac{dL1_{tb}}{dt} = k_{l1} L_{tb}\Omega_i(M1_{tb}; L2_{tb}, L2_1^{\infty}) - d_l L1_{tb} \tag{21}$$

$$\frac{dL2_{tb}}{dt} = k_{l2} L_{tb}\Omega_i(M2_{tb}; F_{tb}, F^{\infty}) - d_l L2_{tb} \tag{22}$$

$$\frac{dF_{tb}}{dt} = s_f + \Omega_i(F_{tb}; N_{tb}, N_2^{\infty}, M1_{tb}, M1_2^{\infty})\left(k_f + \alpha_{dam} Dam_{tb} + \alpha_{m2} M2_{tb}\right) - d_f F_{tb} \tag{23}$$

where the functions used on the right-hand sides of these equations are given by the following:

$$B_n(G_{bm}^{*},\ G_{bm}^{**}, \bar{N}_{bv}, \bar{N}_{tb}) = \frac{\alpha_n}{1 + \beta_n(G_{bm}^{*} + \theta_{nbm} G_{bm}^{**} + \theta_{nbv}\bar{N}_{bv} + \theta_{ntb}\bar{N}_{tb})}, \tag{24}$$

$$B_m(M_{bm}^{*},\ M_{bm}^{**}, \bar{M}_{bv}, \bar{M}_{tb}) = \frac{\alpha_m}{1 + \beta_m(M_{bm}^{*} + \theta_{mbm} M_{bm}^{**} + \theta_{mbv}\bar{M}_{bv} + \theta_{mtb}\bar{M}_{tb})}, \tag{25}$$

$$B_l(L_{bm}^{*}, L_{lt}^{**}, \bar{L}_{bv}) = \frac{\alpha_l}{1 + \beta_l(L_{bm}^{*} + \theta_{llt} L_{lt}^{**} + \theta_{lbv}\bar{L}_{bv})}, \tag{26}$$

$$\Delta_n(\bar{N}_{bv}) = \delta_{n0}\frac{1+\zeta_{n1}\bar{N}_{bv}}{1 + \zeta_{n2}\bar{N}_{bv}} \quad \text{with } \zeta_{n1} < \zeta_{n2}, \tag{27}$$

$$\Delta_m(\bar{M}_{bv}) = \delta_{m0}\frac{1+\zeta_{m1}\bar{M}_{bv}}{1 + \zeta_{m2}\bar{M}_{bv}} \quad \text{with } \zeta_{m1} < \zeta_{m2}, \tag{28}$$

$$\Omega_i(X; Y_1, Y_1^{\infty}, \ldots, Y_m, Y_m^{\infty}) = \frac{X}{1 + \left(\frac{Y_1}{Y_1^{\infty}}\right)^2 + \ldots + \left(\frac{Y_m}{Y_m^{\infty}}\right)^2}, \tag{29}$$

$$\Omega_H(X, n, X_H) = \frac{X^n}{X_H^n + X^n} \tag{30}$$

$$R_n = \Omega_i(k_{nd} Deb_{tb} + k_{nn} N_{tb} + k_{nm1} M1_{tb}; M2_{tb}, M2^{\infty}, L2_{tb}, L2_1^{\infty}), \tag{31}$$

$$R_{m1} = \Omega_i(k_{m1d} Deb_{tb} + k_{m1n} N_{tb} + k_{m1m1} M1_{tb} + k_{m1l1} L1_{tb}; M2_{tb}, M2^{\infty}, L2_{tb}, L2_1^{\infty}), \tag{32}$$

$$R_{m2} = \Omega_i(k_{m2m1} M1_{tb} + k_{m2m2} M2 + k_{m2l2} L2; N_{tb}, N_1^{\infty}, M1_{tb}, M1_1^{\infty}, F_{tb}, F^{\infty}). \tag{33}$$

All parameters are assumed to be non-negative. Parameter values are discussed in Section 5.

## 4.3 Model Processes

The following subsections describe the processes within the TDPM and their interaction.

### 4.3.1. State variable transitions and interactions

State variable transitions and interactions within and across the bone marrow, lymphatic tissues, and blood vessels primarily mimic the processes by which mature hematopoietic cells (granulocytes, monocytes, and lymphocytes) are generated by hematopoietic stem cells (HSCs). Here, we adopt the model formulation presented in (Smirnova 2012), which is also currently implemented in HENRE, to describe the hematopoietic subsystem of the TDPM.

Tissue damage caused by thermal insult can also activate hematopoietic progenitors in addition to other systemic effects (Yang et al. 2011; Valvis et al. 2015; Yáñez et al. 2017). However, these dynamics are not currently incorporated into the model, as we wish to reproduce wound healing following superficial injury, which is characterized by a local response. However, in the future, we plan to extend the TDPM to account for these effects.

### 4.3.2. Progenitors

HSCs give rise to two types of common progenitors[6]: myeloid and lymphoid (Murphy and Weaver 2017). In the bone marrow, common myeloid progenitors produce granulocytes and monocytes via a sequence of progenitor differentiation (Blumenreich 1990). The classical view of hematopoiesis assumes progenitors remain mostly pluripotent (Yáñez et al. 2017) (i.e., capable of differentiating to multiple types of cells), however, recent studies suggest that lineage commitment to a single cell type occurs earlier (Paul et al. 2015; Notta et al. 2016). As a result, we assume different progenitor lineages for granulocytes and monocytes, denoted by $N_{bm}^{c}$ $and$ $M_{bm}^{c}$ for $c = *, **$.

Activated in effort to maintain homeostasis of the granulopoiesis system (Yáñez et al. 2017) ($G_{bm}^{*}$, $G_{bm}^{**}$, $\bar{N}_{bv}$, $and$ $\bar{N}_{tb}$), progenitor maturation involves a high proliferation period ($G_{bm}^{*}$) followed by another in which mitosis no longer occurs ($G_{bm}^{**}$) (Smirnova 2012). As defined in Equation (1), the granulocyte progenitor proliferation rate, denoted by $B_n(\cdot)$, is assumed to be a function of $G_{bm}^{*}$, $G_{bm}^{**}$, $\bar{N}_{bv}$, and $\bar{N}_{tb}$ to reflect that this response aims to keep the system in homeostasis; that is, when any one or more of cell populations in the granulopoiesis system experience a significant depletion, $B_n(\cdot)$ increases towards $\alpha_n$, the maximum granulocyte repopulation rate, to quickly repopulate the affected compartment(s). On the other hand, when cellular populations are near or above their hemostatic levels, $B_n(\cdot)$ decreases, converging to zero.

### 4.3.3. Mitogenic to post-mitogenic transition

The transition rate from mitogenic ($G_{bm}^{*}$) to post-mitogenic ($G_{bm}^{**}$) is given by the second term $\eta_{bmbm}G_{bm}^{*}$ in Equation (1), where $1/\eta_{bmbm}$ corresponds to the mean length of time a progenitor spends in proliferation. Once maturation is complete, $G_{bm}^{**}$ differentiate and enter the bloodstream as mature, inactivated granulocytes ($\bar{N}_{bv}$). The term $\Delta_n(\bar{N}_{bv})G_{bm}^{**}$ describes the influx rate of $G_{bm}^{**}$ into the blood vessels where the function $\Delta_n(\cdot)$, which is defined in Equation (26), scales the granulocyte supply in response to $\bar{N}_{bv}$ in a monotonically decreasing manner. To see this, define $h(\bar{N}_{bv})$ to be the fraction term in $\Delta_n(\cdot)$, i.e., $h(\bar{N}_{bv}) \coloneqq \frac{1+\zeta_{n1}\bar{N}_{bv}}{1+\zeta_{n2}\bar{N}_{bv}}$. Observe the following:

- when $\bar{N}_{bv} = 0$, then $h(0) = 1$ and $\Delta_n(0) = \delta_{n0}$; and
- as $\bar{N}_{bv} \to \infty$, then $h \to \zeta_{n1}/\zeta_{n2}$ and $\Delta_n \to \frac{\delta_{n0}\zeta_{n1}}{\zeta_{n2}}$.

Since $\zeta_{n1} < \zeta_{n2}$, it follows that $\delta_{n0} > \delta_{n0}\zeta_{n1}/\zeta_{n2}$. Whence, as granulocytes in circulation increases, the influx rate of newly matured granulocytes from the bone marrow decreases. Although "granulocytes" is a collective term for neutrophils, eosinophils, and basophils, here we only consider neutrophils. Consequently, resting granulocytes (neutrophils) remain in circulation until they are recruited to the wound site or die naturally (see terms $\bar{\eta}_{bvtb}\bar{N}_{bv}$ and $\bar{d}_n\bar{N}_{bv}$, respectively, in Equation (11)) (Murphy and Weaver 2017).

Since the sequence of cellular events characterizing monopoiesis- the process by which mature monocytes are produced within the bone marrow- parallels that for granulopoiesis, we do not detail its model representation, but note that the corresponding state variables and parameters possess analogous meanings for monocytes. Originating in the bone marrow as common lymphoid progenitors (Murphy and Weaver

[6] HSCs and progenitors share many similarities, including the ability to divide via mitosis. However, HSCs can do so indefinitely whereas division for progenitors is limited (Fuchs and Chen 2013).

2017), mature naïve[7] lymphocytes follow a similar development process as neutrophils and monocytes with several distinctions. As a result, the equations describing lymphopoieses strongly mirror those for granulopoiesis with analogous representations in terms of $L$, and *we only highlight those variables and expressions distinct from the other hematopoietic subsystems*. Moreover, while lymphocytes produce several kinds of cells, we only consider T-cells/T lymphocytes.

While granulocyte and monocyte progenitors remain in the bone marrow throughout maturation (Dicarlo et al. 2020), only mitogenic lymphocyte precursors[8] ($L_{bm}^{*}$) reside in the bone marrow, migrating to the thymus ($L_{lt}^{**}$) where are no longer able to proliferate (Luckheeram et al. 2012). Unlike neutrophils, mature naïve T-cells recirculate through the peripheral lymphatic tissues/bloodstream (Murphy and Weaver 2017), which is modeled with the linear terms $\bar{\lambda}_{bvlt}\bar{L}_{bv}$ and $\bar{\lambda}_{ltbv}\bar{L}_{lt}$, where $1/\bar{\lambda}_{ij}$ denotes the average amount of time $\bar{L}_i$ spends in compartment $i$ before migrating to compartment $j$. For example, a mature naïve T-cell spends approximately 30 minutes in the bloodstream versus 12 hours in the lymph nodes (Prendergast and Jaffee 2013; Owen et al. 2019). Since naïve T-cells do not strictly remain in circulation, we need not describe the influx of mature naïve cells from the thymus using a saturating function as was done for the granulocyte system, i.e., $\Delta_n$. Instead, we use the term $\lambda_{ltbv}L_{lt}^{**}$ to describe the transition rate of $L_{lt}^{**}$ to $\bar{L}_{bv}$ where $1/\lambda_{ltbv}$ can be interpreted the same as $1/\bar{\lambda}_{ij}$.

### 4.3.4. Recruitment of neutrophils and monocytes/macrophages by the burn site

Following injury, circulating neutrophils ($\bar{N}_{bv}$) and monocytes ($\bar{M}_{bv}$) are recruited to the thermal burn site at rates $\bar{\eta}_{bvtb}$ and $\bar{\mu}_{bvtb}$ (see Equations (11) and (12)). Upon arrival, both are activated by signaling biomolecules residing in the local environment (Goldberg and Diegelmann 2010; Schultz et al. 2011). We assume neutrophil activation is initiated by local debris via damage-associated molecular patterns and proinflammatory mediators released by other neutrophils and pro-inflammatory M1 macrophages. Since we do not explicitly account for these mediators in the model, we use $Deb_{tb}$, $N_{tb}$, and $M1_{tb}$ as surrogate metrics for levels (Segal et al. 2012). Slightly modifying the approaches of Reynolds, et al. (Reynolds et al. 2006) and Menke, et al. (Menke et al. 2010), anti-inflammatory signaling biomolecules produced by $M2_{tb}$ and $L2_{tb}$ inhibit neutrophil activation rate. The overall rate with the effects of inhibition is defined in $R_n$ (see Equation (31)). The terms $-k_{nm1p}N_{tb}\Omega_i(M1_{tb}; N_{tb}, N_1^{\infty})$ and $-k_{nm2p}N_{tb}\Omega_i(M2_{tb}; N_{tb}, N_1^{\infty})$ where the function $\Omega_i(\cdot\,;\cdot)$ is given in Equation (29) are added to the expression for $dN_{tb}/dt$ (see Equation (16)), accounting for phagocytic behavior of macrophages to clear (apoptotic) neutrophils. Apoptotic neutrophils are not modeled explicitly. Therefore, their removal from the local wound site is accounted for directly in the removal of $N_{tb}$(Goldberg and Diegelmann 2010).

Similarly, signaling molecules present in the wound environment, debris, and other stimuli trigger resting monocytes and tissue-resident macrophages ($\bar{M}_{tb}$) to differentiate into either M1 macrophages ($M1_{tb}$) or M2 macrophages ($M2_{tb}$) (Hesketh et al. 2017). In the early stages of monocyte/macrophage recruitment and migration, monocytes and tissue-resident macrophages preferentially activate into $M1_{tb}$ due to the pro-inflammatory conditions triggered by damaged tissue, debris, neutrophils, and signaling molecules of M1 macrophages, and L1 T lymphocytes (Hesketh et al. 2017). Accounting for the inhibitory effects procured by $M2_{tb}$ and $L2_{tb}$ via their anti-inflammatory biomolecules, we assume $M1_{tb}$ activation occurs at a rate of $R_{m1}$, which is explicitly defined in Equation (32). Applying similar reasoning to M2 macrophage activation at the location of the thermal burn, $R_{m2}$ is used to describe its corresponding rate (see Equation (33)). $R_{m2}$ also includes inhibition by $F_{tb}$ to sure that $M2_{tb}$ clears as the proliferative phase accelerates

[7] For mature lymphocytes, naïve refers to those cells who have yet to encounter its activating antigen (Prendergast and Jaffee 2013).

[8] The delineating feature between progenitor and precursor cells is the ability of the former to differentiate into many cell types whereas the latter can only differentiate into one.

(Menke et al. 2010). Since macrophages can shift between the M1 and M2 phenotypes during wound healing process (Krzyszczyk et al. 2018), we add (subtract) $\theta_{m1m2}\,[k_{nm1p}N_{tb}\Omega_i(M1_{tb};N_{tb},N_1^{\infty})]$ and subtract (add) $k_{m2m1}M2_{tb}$ to the equation for $dM2_{tb}/dt$ ($dM1_{tb}/dt$). Note that the transition rate from $M1_{tb}$ to $M2_{tb}$ is assume to be proportional to phagocytic rate of $N_{tb}$ by $M1_{tb}$ (Torres et al. 2019), which captures the removal of apoptotic neutrophils by M1 macrophages that is known to promote this phenotype transition. This representation also ensures switching between the macrophage phenotypes is strongly preferential towards $M2_{tb}$ (Hesketh et al. 2017).

### 4.3.5. Fibroblast activity in the proliferation phase

To capture early fibroblast activity of the proliferation phase of wound healing, we build from the modeling approaches of Segal, et al. (Segal et al. 2012) and Menke, et al. (Menke et al. 2010). In Equation (23), we assume non-injury recruitment of fibroblasts from the surrounding tissues occurs as a constant rate of $s_f$, producing a consistent level of fibroblasts known to be present in both pre-damaged and healed wounds (Segal et al. 2012), (Menke et al. 2010). In the absence of injury and thereby, inflammation/repair, the rate of fibroblast proliferation and activation is taken to be proportional to its cell population level giving rise to the term $k_f F_{tb}$. However, active pro-inflammatory cells, such as $N_{tb}$ and $M1_{tb}$, destroy $F_{tb}$ as well as secrete other stimuli that inhibit fibroblast recruitment (Van Linthout et al. 2014),(Menke et al. 2007). Due to the ability of $M2_{tb}$ to produce signaling molecules that foster an anti-inflammatory environment aimed at suppressing inflammatory responses and progressing to repair, $M2_{tb}$ amplifies the fibroblast activity; to model this effect, we introduce the multiplier $(\alpha_{m2}\,M2_{tb})$. An additional multiplier, $\alpha_{dam}Dam_{tb}$, is incorporated to reflect that fibroblast proliferation and activation will also be affected by the amount of damage tissue. Let $(k_f\ + \alpha_{m2}\,M2_{tb} + \alpha_{dam}Dam_{tb})$ be denoted by $s$. Observe that when $M2_{tb}$ and $Dam_{tb}$ equal zero, $s$ is $k_f$, corresponding to the situation where fibroblast activation and proliferation is unaffected. That is, when no M2 macrophages are present at the wound site and there is also no damaged tissue. Now, if $M2_{tb}$>0 and/or $Dam_{tb} > 0$, $s$ is strictly greater than $k_f$, and $M2_{tb}/Dam_{tb}$ increases fibroblast activity. Incorporating all of these components, the updated rate of activation and proliferation for $F_{tb}$ is given by $\Omega_i(F_{tb};N_{tb},N_2^{\infty},M1_{tb},M1_2^{\infty})\big(k_f + \alpha_{dam}Dam_{tb} + \alpha_{m2}M2_{tb}\big)$, where the inhibition function $\Omega_i(\cdot)$ is defined in Equation (29).

The final terms of $dN_{tb}/dt$, $dM1_{tb}/dt$, $dM2_{tb}/dt$ and $dF_{tb}/dt$ (see Equations (15), (17)-(19)) account for the intrinsic decay of activated neutrophils, activated M1 macrophages, activated M2 macrophages, and fibroblasts, respectively, noting that $d$ is employed to represent the different decay rates in the model with the name notation conventions mentioned earlier. In ODE models, intrinsic decay values typically correspond to estimates obtained using half-lives of cells (Reynolds et al. 2006) and, unless stated otherwise, we also adopt this approach.

### 4.3.6. T lymphocyte activation

Following injury, naïve T lymphocyte activation via antigen presentation by migratory dendritic cells must occur in the peripheral lymphatic tissues (Alberts et al. 2002). Naïve lymphocytes that fail to encounter their associated antigen, and therefore remain naïve, re-enter the bloodstream where they continue circulating between peripheral lymphatic tissues ($\bar{L}_{lt}$) and blood vessels ($\bar{L}_{bv}$) until they recognize an antigen ($\bar{\lambda}_{ltbv}\bar{L}_{lt}$ and $\bar{\lambda}_{bvlt}\bar{L}_{bv}$) or naturally die (see terms $\bar{d}_l\bar{L}_{lt}$ and $\bar{d}_l\bar{L}_{bv}$) (Alberts et al. 2002). On the other hand, rather than immediately migrating to the thermal burn site, activated T-cells ($L_{lt}$) must remain in the peripheral tissues where they undergo a period of proliferation and differentiation (Murphy and Weaver 2017). The term $\rho_l L_{lt}$ is added to the $dL_{lt}/dt$ (see Equation (8)) to account for this process.

It has been observed that while initial T-cell activation and various degrees of differentiation take place in the peripheral lymphatic tissues, additional differentiation and amplification into pro-inflammatory ($L1_{tb}$) and anti-inflammatory ($L2_{tb}$) functions can occur upon arrival at the local wound due to the presence of

signaling biomolecules in the environment produced by $M1_{tb}$ and by $M2_{tb}$ (Mills and Ley 2014; Murphy and Weaver 2017; Torres et al. 2019). To incorporate these dynamics into the model, the term $-\bar{\bar{\lambda}}_{ltlt}\bar{L}_{lt}$ is added (subtracted) to the equation for $d\bar{L}_{lt}/dt$ ($dL_{lt}/dt$) (refer to Equations (7) and (8)). Activated T lymphocytes then enter the blood vessels and wound site at rates of $\lambda_{ltbv}L_{lt}$ and $\lambda_{bvtb}L_{bv}$, respectively. Upon arrival at the site of injury, $L_{tb}$ differentiates into $L1_{tb}$ and $L2_{tb}$ according to $k_{l1}L_{tb}\Omega_i(M1_{tb}; L2_{tb}, L2_1^{\infty})$ and $k_{l2}L_{tb}\Omega_i(M2_{tb}; F_{tb}, F^{\infty})$, respectively. Observe that the first rate also includes inhibition by $L2_{tb}$ due to its anti-inflammatory biomolecules. Similarly, the inhibition in the rate for $L2_{tb}$ by $F_{tb}$ is included to ensure resolution of the anti-inflammatory cascade as the proliferative phase revs up. Like other immune cell equations, the last term in each of the lymphocyte ODEs, excluding $dL_{lt}/dt$, incorporates the decay rate of the population.

### 4.3.7. Damaged tissue and Debris

Damaged tissue ($Dam_{tb}$), which corresponds to Equation (13), results from not only from the thermal burn wound, but also collateral damage due to proteases and other tissue degrading molecules produced by $N_{tb}$ and $M1_{tb}$ at the injury site (Schultz et al. 2011; Namas et al. 2015; Goldberg and Diegelmann 2020). It is assumed that this increase in damaged tissue also creates further debris, $Deb_{tb}$, hence the appearance of the same first two terms in the equations for $Dam_{tb}$ and $Deb_{tb}$ (see Equation (14). Note that $M2_{tb}$ does not contribute to this process. Tissue damage releases more pro-inflammatory molecules that recruit more immune cells, creating a positive feedback loop between $D_{tb}$ and $N_{tb}/M1_{tb}$ (Menke et al. 2010; Namas et al. 2015).

Following the approach in (Reynolds et al. 2006; Menke et al. 2010), this process does not occur exponentially but instead saturates, hence the inclusion of a Hill function, dynamics via the function $\Omega_H(\cdot;\cdot)$ as defined according to Equation (30). In assigning an exponential value of six in $\Omega_s$, low population levels of neutrophils and macrophages are unable to cause significant damage (Menke et al. 2010). Inhibition by $L2_{tb}$ was incorporated into $\Omega_H$ in order to account for inhibition from biomolecules produced by regulatory T lymphocytes, Tregs, in preventing further tissue degradation (Murphy and Weaver 2017). The final two terms in expression for $dDam_{tb}/dt$ (see Equation (13)), $\rho_{dam}\Omega_i(Dam_{tb}; Deb_{tb}, Deb_{dam}^{\infty})$ and $k_{df}F_{tb}\Omega_i(Dam_{tb}; Deb_{tb}, Deb_{dam}^{\infty})$, represent intrinsic and fibroblast-related tissue repair, respectively. Both are assumed to be inhibited by $Deb_{tb}$ to ensure repair of damaged tissue cannot occur until debris has been cleared from the wound site.

The third, fourth, and fifth terms of the $Deb_{tb}$ equation (see Equation (14) reflect phagocytosis of debris by neutrophils and macrophages. As mentioned before, $N_{tb}$ interferes with the phagocytic activity of $M1_{tb}$ and $M2_{tb}$ via reactive oxygen species, hence the inclusion of the inhibitory function. The last terms accounts for removal of debris by other inflammatory cells at the burn site.

# Section 5. Reduced Time-Dependent Physiological Model for Superficial Thermal Burns

However, while inflammatory mediators are also released at the superficial thermal burn site, this release does not spillover into circulation resulting in no systemic effects (Hettiaratchy and Dziewulski 2004; Wang 2014). Thus, it is assumed that superficial injury does not result in significant perturbations to innate and adaptive immune responses beyond the local wound site. Mathematically, this equates to cellular dynamics in the bone marrow, lymphatic tissues and blood vessels being sufficiently constant for all of time, or equivalently, each of the derivatives in Equations (1)-(12) being equal to zero; this is commonly referred as a quasi-steady state assumption. It follows that the recruitment/influx terms in Equations (15), (17), and (20) are also constant, allowing us to set production and recruitment rates to the following constant values:

$$s_{nr} = \bar{\eta}_{bvtb}\,\bar{N}_{bv}, \qquad s_{mr} = \bar{\mu}_{bvtb}\,\bar{M}_{bv}, \qquad s_{lr} = \lambda_{bvtb} L_{bv}, \tag{34}$$

where $s_{cr} \geq 0$ for $c = n, m, l$.

Additionally, activation of resting neutrophils and monocytes and differentiation of activated T-cell lymphocytes at the local wound site occurs rapidly, especially relative to the time scale of other interactions (Reynolds et al. 2006). Hence, we again apply the quasi-steady state assumption to variables $\bar{N}_{tb}$, $\bar{M}_{tb}$, and $L_{tb}$, i.e., $\frac{d\bar{N}_{tb}}{dt} = \frac{d\bar{M}_{tb}}{dt} = \frac{dL_{tb}}{dt} = 0$, with (23) to obtain

$$\bar{N}_{tb} = \frac{s_{nr}}{R_n + d_{nr}}$$

$$\bar{M}_{tb} = \frac{s_{mr}}{R_{m1} + R_{m2} + d_{mr}}$$

$$L_{tb} = \frac{s_{lr}}{k_{l1}\Omega_i(M1_{tb}; L2_{tb}, L2_1^{\infty}) + k_{l2}\Omega_i(M2_{tb}; F_{tb}, F^{\infty}) + d_{lr}}$$

respectively.

Whence, to study the inflammatory and early fibroblast activity of wound healing following a superficial thermal burn, it suffices to consider a reduced form of the full TDPM given by

$$\begin{aligned}\frac{dDam_{tb}}{dt} = {} & k_{dn}\Omega_H(\Omega_i(N_{tb}; L2_{tb}, L2_2^{\infty}), 6, N_H) + \sigma_{m1}k_{dn}\Omega_H(\Omega_i(M1_{tb}; L2_{tb}, L2_2^{\infty}), 6, M1_H) \\ & - \rho_{dam}\Omega_i(Dam_{tb}; Deb_{tb}, Deb_{dam}^{\infty}) - k_{df}F_{tb}\Omega_i(Dam_{tb}; Deb_{tb}, Deb_{dam}^{\infty})\end{aligned} \tag{35}$$

$$\begin{aligned}\frac{dDeb_{tb}}{dt} = {} & k_{dn}\Omega_H(\Omega_i(N_{tb}; L2_{tb}, L2_2^{\infty}), 6, N_H) + \sigma_{m1}k_{dn}\Omega_H(\Omega_i(M1_{tb}; L2_{tb}, L2_2^{\infty}), 6, M1_H) \\ & - k_{dnp}N_{tb}\Omega_H(Deb_{tb}, 1, Deb_H) - k_{dm1p}\Omega_i(M1_{tb}; N_{tb}, N_1^{\infty})\Omega_H(Deb_{tb}, 1, Deb_H) \\ & - k_{dm2p}\Omega_i(M2_{tb}; N_{tb}, N_1^{\infty})\Omega_H(Deb_{tb}, 1, Deb_H) - d_{deb}Deb_{tb}\end{aligned} \tag{36}$$

$$\frac{dN_{tb}}{dt} = \frac{s_{nr}R_n}{R_n + d_{nr}} - k_{nm1p}N_{tb}\Omega_i(M1_{tb}; N_{tb}, N_1^{\infty}) - k_{nm2p}N_{tb}\Omega_i(M2_{tb}; N_{tb}, N_1^{\infty}) - d_nN_{tb} \tag{37}$$

$$\frac{dM1_{tb}}{dt} = \frac{s_{mr}R_{m1}}{R_{m1} + R_{m2} + d_{mr}} - \theta_{m1m2}\,[k_{nm1p}N_{tb}\Omega_i(M1_{tb}; N_{tb}, N_1^{\infty})] + \theta_{m2m1}M2_{tb} - d_{m1}M1_{tb} \tag{38}$$

$$\frac{dM2_{tb}}{dt} = \frac{s_{mr}R_{m2}}{R_{m1} + R_{m2} + d_{mr}} + \theta_{m1m2}\,[k_{nm1p}N_{tb}\Omega_i(M1_{tb}; N_{tb}, N_1^{\infty})] - \theta_{m2m1}M2_{tb} - d_{m2}M2_{tb} \tag{39}$$

$$\frac{dL1_{tb}}{dt} = \frac{s_{lr} k_{l1} \Omega_i(M1_{tb}; L2_{tb}, L2_1^{\infty})}{k_{l1} \Omega_i(M1_{tb}; L2_{tb}, L2_1^{\infty}) + k_{l2} \Omega_i(M2_{tb}; F_{tb}, F^{\infty}) + d_{lr}} - d_l L1_{tb} \tag{40}$$

$$\frac{dL2_{tb}}{dt} = \frac{s_{lr} k_{l2} \Omega_i(M2_{tb}; F_{tb}, F^{\infty})}{k_{l1} \Omega_i(M1_{tb}; L2_{tb}, L2_1^{\infty}) + k_{l2} \Omega_i(M2_{tb}; F_{tb}, F^{\infty}) + d_{lr}} - d_l L2_{tb} \tag{41}$$

$$\frac{dF_{tb}}{dt} = s_f + \Omega_i(F_{tb}; N_{tb}, N_2^{\infty}, M1_{tb}, M1_2^{\infty})\left(k_f + \alpha_{dam} Dam_{tb} + \alpha_{m2} M2_{tb}\right) - d_f F_{tb} \tag{42}$$

Where the auxiliary functions are defined as in Equations (29)-(33) above. We remark that while the equations for tissue damage, $Dam_{tb}$, debris, $Deb_{tb}$, and activated/proliferating fibroblasts, $F_{tb}$, do not differ from those in the full TDPM system, they are intentionally duplicated to present the reduced TDPM in its entirety.

# Section 6. Numerical Simulations

Numerical simulations of the reduced TDPM governed by Equations (37)-(43) were performed to display known and feasible biological behavior following superficial thermal burns. We first establish normal wound healing dynamics produced by the model, which we refer to as our baseline case. Parameters were primarily obtained from the existing literature (Reynolds et al. 2006; Menke et al. 2010; Segal et al. 2012; Day et al. 2015; Cooper et al. 2015; Torres et al. 2019)and their assigned (baseline) values are provided in Table 2 and Table 3. However, we performed additional calibration of these values to ensure the wound healed in a specified time frame. We then conducted additional experiments involving perturbations of the parameters of the model to reflect known environmental or biological phenomena, and each were assessed for their effect on baseline normal wound-healing dynamics.

Adopting an analogous definition of Menke, et al. (Menke et al. 2010), the burn wound is said to be *healed* when $Dam_{tb} < 0.01$ (Lateef et al. 2019). Any wounds that do not satisfy this requirement are characterized as *delayed healing*. All numerical simulations were implemented in MATLAB (2020).

**Table 2. Baseline Initial Conditions for Reduced TPDM Given By (35)-(42).**

| SYMBOL | INITIAL CONDITION | |
|---|---|---|
| | Superficial Thickness | Superficial Partial Thickness |
| $\boldsymbol{Dam_{tb}(0)}$ | 0.1 | 0.9 |
| $\boldsymbol{Deb_{tb}(0)}$ | 0.1 | 0.9 |
| $\boldsymbol{N_{tb}}(0)$ | 0 | 0 |
| $\boldsymbol{M1_{tb}(0)}$ | 0 | 0 |
| $\boldsymbol{M2_{tb}(0)}$ | 0 | 0 |
| $\boldsymbol{F_{tb}(0)}$ | 0 | 0 |
| $\boldsymbol{L1_{tb}(0)}$ | 0 | 0 |
| $\boldsymbol{L2_{tb}}(0)$ | 0 | 0 |

**Table 3. Description and Assigned Baseline Values for Parameters of Reduced TPDM Given by Equations (37)-(42).**

| PARAMETER | | DESCRIPTION | UNITS | BASELINE VALUE |
|---|---|---|---|---|
| *Inhibition* | $Deb_{dam}^{\infty}$ | Constant controlling the effectiveness of $Deb_{tb}$ at inhibiting damage repair | $D$-units | 0.01 |
| | $Deb_H$ | Constant controlling the effectiveness of $Deb_{tb}$ at inhibiting phagocytic removal of debris by $N_{tb}$, $M1_{tb}$, and $M2_{tb}$ | $D$-units | 0.0713756 |
| | $N_1^{\infty}$ | Constant controlling the effectiveness of $N_{tb}$ at inhibiting the activity on other immune cells | $N$-units | 0.264838 |
| | $N_2^{\infty}$ | Constant controlling the effectiveness of $N_{tb}$ at inhibiting proliferation and activation of $F_{tb}$ | $N$-units | 0.1 |
| | $M1_1^{\infty}$ | Constant controlling the effectiveness of $M1_{tb}$ at inhibiting activation of $M2_{tb}$ | $M$-units | 0.147243 |
| | $M1_2^{\infty}$ | Constant controlling the effectiveness of $M1_{tb}$ at inhibiting proliferation and activation of $F_{tb}$ | $M$-units | 0.0375 |
| | $M2^{\infty}$ | Constant controlling the effectiveness of $M2_{tb}$ at inhibiting activation of $N_{tb}$ and $M1_{tb}$ | $M$-units | 0.18667 |
| | $F^{\infty}$ | Constant controlling the effectiveness of $F_{tb}$ at inhibiting the activation of $M2_{tb}$ and $L2_{tb}$ | $F$-units | 0.53137 |
| | $L2_1^{\infty}$ | Constant controlling the effectiveness of $L2_{tb}$ at inhibiting the activation of $N_{tb}$, $M1_{tb}$, and $L1_{tb}$ | $L$-units | 0.21395 |
| | $L2_2^{\infty}$ | Constant controlling the effectiveness of $L2_{tb}$ at inhibiting collateral damage associated with $N_{tb}$ and $M1_{tb}$ | $L$-units | 0.12 |
| *Damage and Debris* | $k_{dn}$ | Maximum collateral tissue damage rate caused by $N_{tb}$ at the local burn site | $D$-units/h | 0.000175 |
| | $k_{dm1}$ | Maximum collateral tissue damage rate caused by $M1_{tb}$ at the local burn site | $D$-units/h | $\sigma_{dm1}k_{dn}$ |

| PARAMETER | | DESCRIPTION | UNITS | BASELINE VALUE |
|---|---|---|---|---|
| | $\sigma_{dm1}$ | Tissue damage scaling coefficient for $M1_{tb}$ | Unitless | 0.5 |
| | $N_H$ | Hill constant for tissue damage associated with $N_{tb}$ | $N$-units | 0.06 |
| | $M1_H$ | Hill constant for tissue damage associated with $M1_{tb}$ | $M$-units | 0.06 |
| | $\rho_{dam}$ | Baseline tissue damage repair rate via a combination of repair, resolution, and regeneration | 1/h | 0.004 |
| | $k_{df}$ | Repair rate on $Dam_{tb}$ by $F_{tb}$ | 1/($F$-units·h) | 0.02 |
| | $k_{dnp}$ | Phagocytosis rate of $Deb_{tb}$ by $N_{tb}$ | $D$-units/($N$-units·h) | 0.0077362 |
| | $k_{dm1p}$ | Phagocytosis rate of $Deb_{tb}$ by $M1_{tb}$ | $D$-units/($M$-units·h) | 0.0073472 |
| | $k_{dm2p}$ | Phagocytosis rate of $Deb_{tb}$ by $M2_{tb}$ | $D$-units/($M$-units·h) | 0.0039117 |
| | $d_{deb}$ | Decay rate of $Deb_{tb}$ | 1/h | 0.0001 |
| *Neutrophils* | $s_{nr}$ | Recruitment rate of circulating neutrophils to the local burn site | $N$-units/h | 0.040971 |
| | $d_{nr}$ | Decay rate of resting neutrophils | 1/h | 0.046577 |
| | $d_n$ | Decay rate of $N_{tb}$ | 1/h | 0.108722 |
| | $k_{nd}$ | Activation rate of resting neutrophils to $N_{tb}$ by $Deb_{tb}$ | 1/($D$-units·h) | 0.225435 |
| | $k_{nn}$ | Activation rate of resting neutrophils to $N_{tb}$ by $N_{tb}$ and its byproducts | 1/($N$-units·h) | 0.0168611 |
| | $k_{nm1}$ | Activation rate of resting neutrophils to $N_{tb}$ by $M1_{tb}$and its byproducts | 1/($M$-units·h) | 0 |
| | $k_{nm1p}$ | Phagocytosis rate of $N_{tb}$ by $M1_{tb}$ | 1/($M$-units·h) | 0.12075 |

| PARAMETER | | DESCRIPTION | UNITS | BASELINE VALUE |
|---|---|---|---|---|
| | $k_{nm2p}$ | Phagocytosis rate of $N_{tb}$ by $M2_{tb}$ | 1/($M$-units·h) | 0.3628333 |
| *Macrophages* | $s_{mr}$ | Recruitment rate of tissue-resident macrophages and circulating monocytes to the local burn site | $M$-units/h | 0.506939667 |
| | $d_{mr}$ | Decay rate of resting monocytes and tissue-resident macrophages | 1/h | 0.014202 |
| | $d_{m1}$ | Decay rate of $M1_{tb}$ | 1/h | 0.066316 |
| | $d_{m2}$ | Decay rate of $M2_{tb}$ | 1/h | 0.077357 |
| | $k_{m1d}$ | Activation rate of resting monocytes and tissue-resident macrophages to $M1_{tb}$ by $Deb_{tb}$ | 1/($D$-units·h) | 0.0045977 |
| | $k_{m1n}$ | Activation rate of resting monocytes and tissue-resident macrophages to $M1_{tb}$ by $N_{tb}$ and its byproducts | 1/($N$-units·h) | 0.0034618 |
| | $k_{m1m1}$ | Activation rate of resting monocytes and tissue-resident macrophages to $M1_{tb}$ by $M1_{tb}$ and its byproducts | 1/($M$-units·h) | 0.000037879 |
| | $k_{m1l1}$ | Activation rate of resting monocytes and tissue-resident macrophages to $M1_{tb}$ by $L1_{tb}$ and its byproducts | 1/($L$-units·h) | 0.00064 |
| | $k_{m2m1}$ | Activation rate of resting monocytes and tissue-resident macrophages to $M2_{tb}$ by $M1_{tb}$ and its byproducts | 1/($M$-units·h) | 0.00686345 |
| | $k_{m2m2}$ | Activation rate of resting monocytes and tissue-resident macrophages to $M2_{tb}$ by $M2_{tb}$ and its byproducts | 1/($M$-units·h) | 0.00067667 |
| | $k_{m2l2}$ | Activation rate of resting monocytes and tissue-resident macrophages to $M2_{tb}$ by $L2_{tb}$ and its byproducts | 1/($L$-units·h) | 0.004996 |
| | $\theta_{m1m2}$ | Transition rate of $M1_{tb}$ to $M2_{tb}$ | $M$-units/$N$-units | 0.6900833 |
| | $\theta_{m2m1}$ | Transition rate of $M2_{tb}$ to $M1_{tb}$ | 1/h | 0 |

| PARAMETER | | DESCRIPTION | UNITS | BASELINE VALUE |
|---|---|---|---|---|
| *Fibroblasts* | $s_f$ | Non-injury recruitment rate of fibroblasts to the local burn site | $F$-units/h | 0.0013889 |
| | $d_f$ | Decay rate of $F_{tb}$ | 1/h | 0.0090909 |
| | $k_f$ | Baseline proliferation and activation rate of $F_{tb}$ | 1/h | 0.0053333 |
| | $\alpha_{m2}$ | Constant controlling the up-regulation of $F_{tb}$ proliferation and activation by $M2_{tb}$ | 1/($M$-units·h) | 0.017673 |
| | $\alpha_{dam}$ | Constant controlling the up-regulation of $F_{tb}$ proliferation and activation by $Dam_{tb}$ | 1/($D$-units·h) | 0.0666667 |
| *T Lymphocytes* | $s_{\ell r}$ | Recruitment rate of circulating activated (effector) T lymphocytes to the local burn site | $L$-units/h | 0.90259 |
| | $d_{\ell r}$ | Decay rate of activated (effector) T lymphocytes | 1/h | 0.0417364 |
| | $k_{l1}$ | Induction rate of activated (effector) T lymphocytes to $L1_{tb}$ by $M1_{tb}$ | 1/($M$-units·h) | 0.004 |
| | $k_{l2}$ | Induction rate of activated (effector) T lymphocytes to $L2_{tb}$ by $M2_{tb}$ | 1/($M$-units·h) | 0.0055977 |
| | $d_\ell$ | Decay rate of $L1_{tb}$ and $L2_{tb}$ | 1/h | 0.0474167 |

Notation: $h$ is hours, the timescale of the model. $D$ represents the units for $Dam_{tb}$ and $Deb_{tb}$, since it is the same for both. $N$, $M$, $F$, and $L$ denote the units of neutrophils ($N_{tb}$), macrophages ($M1_{tb}$ and $M2_{tb}$), fibroblasts ($F_{tb}$), and T lymphocytes ($L1_{tb}$ and $L2_{tb}$), respectively.

### 6.1 "Normal" Healing Dynamics

The normal healing process of superficial thickness and partial superficial thickness thermal burn typically resolves in about 3 to 6 days, and 7-14 days, respectively (Peng et al. 2006; Lateef et al. 2019; Abazari et al. 2020). For this work, we are less focused on achieving specific temporal trends than on qualitatively matching the patterns of normal wound healing dynamics (i.e., neutrophil peak followed by macrophage peak). Figure  compares healing dynamics predicted by the model for a superficial thickness burn and the more severe superficial partial thickness, where initial conditions for both injuries are provided in Table 2. Observe that the more severe injury there is an amplified immune response and greater time to healing as expected. The specific healing times are 6.058 days and 13.930 days for the superficial thickness and partial superficial thickness burns, respectively; note that these healing times also fall within the observed ranges.

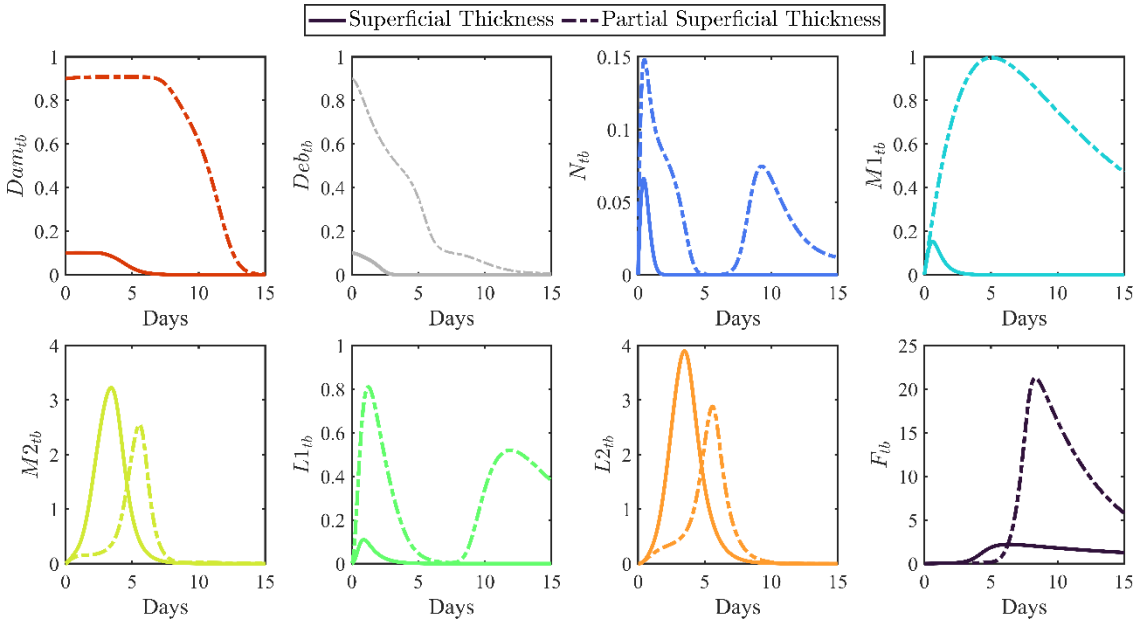


**Figure 2. Baseline (Normal) Healing Dynamics for Superficial Thermal Burns.**

## 6.2 Healing Without Removal of Debris

Assuming a superficial thickness burn, we examined healing dynamic predicted by the model if inflammatory cells could no longer remove $Deb_{tb}$. The transients under baseline parameters compared to when debris remains present in the burn are shown in Figure 3. As desired (following from the definition of the inflammatory phase), when the removal of debris is blocked, the burn does not heal and inflammation is sustained. While this is not the case for the superficial injuries considered in this TR, it is important to verify that the model permits the existence of such solutions.

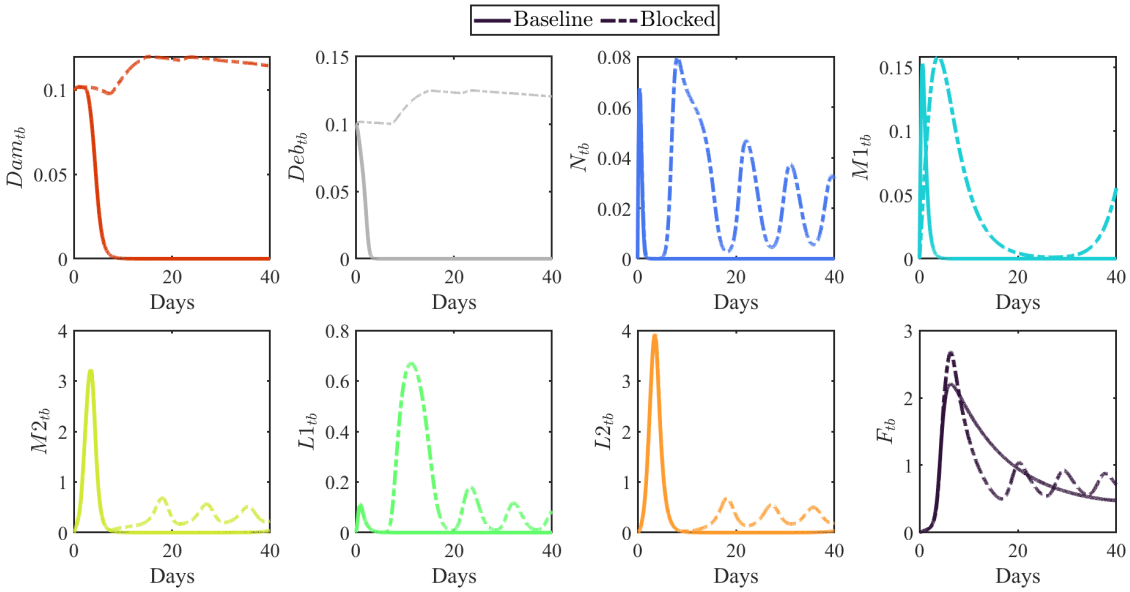


**Figure 3. Transients for numerical simulations when removal of debris is inhibited (dashed line) compared to baseline normal healing dynamics (solid line).**

# Section 7. Discussion

Once initiated, the wound healing process proceeds through a complex sequence of coordinated and overlapping phases to restore anatomic structure and function of the wounded tissues. Timely and efficient progression towards healing hinges upon reaching various immune and inflammatory milestones, which when delayed heightens the risk of an individual's downstream adverse health outcomes like secondary infections, sepsis, and multiple organ dysfunction syndrome. To build a mathematical model of the wound healing cascade activated by thermal burn injury, we first need to understand the "simplest" wound where healing always occurs in the absence of treatment for a healthy individual. Consequently, this report only considered superficial thermal burns.

We presented a TDPM governed by 23 ODEs that capture both hematopoietic and immunologic events across the bone marrow, lymphatic tissues, blood vessels and local wound site. The TDPM linked existing HENRE models for granulopoietic and lymphopoietic cell kinetics with a novel immune-physiological model that describes interactions at the thermal burn site between tissue damage, neutrophils, macrophages, lymphocytes and fibroblasts; it is worth noting that this amalgamation of legacy and freshman models signified an important advancement in the development of a comprehensive, integrative framework in HENRE. An application of the quasi-steady state assumption to the systemic compartments reduced the TDPM to eight equations corresponding to local wound dynamics. A detailed description of the individual terms of the reduced model and their relationship to known physiological behaviors was also provided.

Baseline values, for the reduced TDPM representing normal healing dynamics were identified from published literature then manually calibrated; for the baseline values, TDPM state variables evolved to a healed end state for initial conditions reflective of a superficial thermal burn. We qualitatively match the transients predicted by the model using observed healing times. Using the time series predictions for the baseline values as the comparator, numerical simulations were performed for the reduced TDPM, allowing us to further verify the biological plausibility of its behaviors.

# Section 8. Future Work

Future TDPM development will center around data collection and parameterization of the model, with the latter driven by the results of structural identifiability and global sensitivity analysis (GSA), both of which will assist in making optimal parameter choices; we are currently vetting a range of GSA methodologies which include but are not limited to Partial Rank Correlation Coefficient, the Extended Fourier Amplitude Sensitivity Test and Sobol's method. Integration of these techniques early in the model development process will provide us with the opportunity to minimize the restrictions imposed by limited human data availability. These restrictions are further reduced by to the potential use of local and systemic measurements- as evidenced by the TDPM state variables- for the parameter estimation process; although it is also worth noting that the state variables represent commonly and easily measured entities. Additionally, we will develop a method to transform the time-series output of the TDPM to predict mortality and morbidity outcomes for combined injury resulting from NUDET exposure. Once the TDPM has been augmented to include a sufficient range of thermal burn severity, we will begin incorporating the systemic and local effects of ionizing radiation exposure.

# Section 9. References


Abazari M, Ghaffari A, Rashidzadeh H, Badeleh SM, Maleki Y. A systematic review on classification, identification, and healing process of burn wound healing. Int J Low Extrem Wounds 1–13; 2020.

Alberts B, Johnson A, Lewis J, Raff M, Roberts K, Walter P. Helper T Cells and Lymphocyte Activation. 4th ed. Garland Science; 2002.

Arnold CE, Barker RN, Wilson HM. Critical role for inflammatory macrophages in driving antigen-dependent Th17Cell responses? J Cytokine Biol 01:1–3; 2016.

Barton GM. A calculated response: Control of inflammation by the innate immune system. J Clin Invest 118:413–420; 2008.

Baue AE, Durham R, Faist E. Systemic inflammatory response syndrome (SIRS), multiple organ dysfunction syndrome (MODS), multiple organ failure (MOF): Are we winning the battle? Shock 10:79–89; 1998.

Blumenreich MS. The White Blood Cell and Differential Count. In: Clinical Methods: The History, Physical, and Laboratory Examinations. Butterworths; 1990.

Buganza Tepole A, Kuhl E. Systems-based approaches toward wound healing. 2013.

Church D, Elsayed S, Reid O, Winston B, Lindsay R. Burn wound infections. Clin Microbiol Rev 19:403–434; 2006.

Čoma M, Fröhlichová L, Urban L, Zajíček R, Urban T, Szabo P, Novák Š, Fetissov V, Dvořánková B, Smetana K, Gál P. Molecular changes underlying hypertrophic scarring following burns involve specific deregulations at all wound healing stages (inflammation, proliferation and maturation). Int J Mol Sci 22:897; 2021.

Cooper RL, Segal RA, Diegelmann RF, Reynolds AM. Modeling the effects of systemic mediators on the inflammatory phase of wound healing. J Theor Biol 367:86–99; 2015.

Day JD, Metes DM, Vodovotz Y. Mathematical modeling of early cellular innate and adaptive immune responses to ischemia/reperfusion injury and solid organ allotransplantation. Front Immunol 6; 2015.

Dicarlo AL, Bandremer AC, Hollingsworth BA, Kasim S, Laniyonu A, Todd NF, Wang SJ, Wertheimer ER, Rios CI. Cutaneous radiation injuries: Models, assessment and treatments. Radiat Res 194:315–344; 2020.

Diegelmann RF, Evans MC. Wound Healing: An overview of acute, fibrotic and delayed healing. Front Biosci 9:283–289; 2004.

Ellis S, Lin EJ, Tartar D. Immunology of wound healing. Curr Dermatol Rep 7:350–358; 2018.

Entezami KZ, Mosavi T. Determination of lymphocytes surface markers in patients with thermal burns and the influence of burn size on mononuclear cell subsets. Med J Islam Repub Iran 31:219–223; 2017.

Evers LH, Bhavsar D, Mailänder P. The biology of burn injury. Exp Dermatol 19:777–783; 2010.

Ferrante CJ, Leibovich SJ. Regulation of macrophage polarization and wound healing. Adv Wound Care 1:10–16; 2012.

Fuchs E, Chen T. A matter of life and death: Self-renewal in stem cells. EMBO Rep 14:39–48; 2013.

Gale AJ. Current understanding of hemostasis. Toxicol Pathol 39:273–280; 2011.

Goldberg SR, Diegelmann RF. Wound healing primer. Surg Clin North Am 90:1133–1146; 2010.

Goldberg SR, Diegelmann RF. What makes wounds chronic. Surg Clin North Am 100:681–693; 2020.

Hesketh M, Sahin KB, West ZE, Murray RZ. Macrophage phenotypes regulate scar formation and chronic wound healing. Int J Mol Sci 18; 2017.

Hettiaratchy S, Dziewulski P. ABC of Burns: Pathophysiology and types of burns. BMJ 328:1427–1429; 2004.

Jeschke MG, van Baar ME, Choudhry MA, Chung KK, Gibran NS, Logsetty S. Burn injury. Nat Rev Dis Prim 6; 2020.

Kotwal GJ, Chien S. Macrophage differentiation in normal and accelerated wound healing. Results Probl Cell Differ 62:353–364; 2017.

Krzyszczyk P, Schloss R, Palmer A, Berthiaume F. The role of macrophages in acute and chronic wound healing and interventions to promote pro-wound healing phenotypes. Front Physiol 9:419; 2018.

Lateef Z, Stuart G, Jones N, Mercer A, Fleming S, Wise L. The cutaneous inflammatory response to thermal burn injury in a Murine model. Int J Mol Sci 20:538; 2019.

Luckheeram RV, Zhou R, Verma AD, Xia B. CD4 + T Cells: Differentiation and functions. Clin Dev Immunol 2012; 2012.

Menke NB, Cain JW, Reynolds A, Chan DM, Segal RA, Witten TM, Bonchev DG, Diegelmann RF, Ward KR. An in silico approach to the analysis of acute wound healing. Wound Repair Regen 18:105–113; 2010.

Menke NB, Ward KR, Witten TM, Bonchev DG, Diegelmann RF. Impaired wound healing. Clin Dermatol 25:19–25; 2007.

Meziani L, Deutsch E, Mondini M. Macrophages in radiation injury: a new therapeutic target. Oncoimmunology 7:e1494488; 2018.

Mills CD, Ley K. M1 and M2 macrophages: The chicken and the egg of immunity. J Innate Immun 6:716–726; 2014.

Murphy K, Weaver C. Janeway's Immunobiology. Garland Science. 2017.

Namas RA, Mi Q, Namas R, Almahmoud K, Zaaqoq AM, Abdul-Malak O, Azhar N, Day J, Abboud A, Zamora R, Billiar TR, Vodovotz Y. Insights into the role of chemokines, damage-associated molecular patterns, and lymphocyte-derived mediators from computational models of trauma-induced inflammation. Antioxidants Redox Signal 23:1370–1387; 2015.

Notta F, Zandi S, Takayama N, Dobson S, Gan OI, Wilson G, Kaufmann KB, McLeod J, Laurenti E, Dunant CF, McPherson JD, Stein LD, Dror Y, Dick JE. Distinct routes of lineage development reshape the human blood hierarchy across ontogeny. Science (80- ) 351:aab2116; 2016.

Orsted HL, Keast D, Forest-lalande L. Basic principles of wound healing. Wound Care Canada 9:1–5; 2016.

Oughterson AW, LeRoy G V., Liebow AA, Hammond EC, Barnett HL, Rosenbaum JD, Schneider BA. Medical Effects Of Atomic Bombs, The Report Of The Joint Commission For The Investigation Of The Effects Of The Atomic Bomb In Japan Volume 1. U.S. Atomic Energy Commission; 1951.

Owen J, Punt J, Stranford S, Kuby J. Kuby Immunology. 8th ed. Macmillan; 2019.

Paul F, Arkin Y, Giladi A, Jaitin D, Kenigsberg E, Keren-Shaul H, Winter D, Lara-Astiaso D, Gury M,

Weiner A, David E, Cohen N, Lauridsen FKB, Haas S, Schlitzer A, Mildner A, Ginhoux F, Jung S, Trumpp A, Porse B, Tanay A, Amit I. Transcriptional heterogeneity and lineage commitment in myeloid progenitors. Cell 163:1663–1677; 2015.

Paulnock DM. Macrophage activation by T cells. Curr Opin Immunol 4:344–349; 1992.

Peng D, Huang W, Ai S, Wang S. Clinical significance of leukocyte infiltrative response in deep wound of patients with major burns. Burns 32:946–950; 2006.

Pinto AT, Pinto ML, Cardoso AP, Monteiro C, Pinto MT, Maia AF, Castro P, Figueira R, Monteiro A, Marques M, Mareel M, Dos Santos SG, Seruca R, Barbosa MA, Rocha S, Oliveira MJ. Ionizing radiation modulates human macrophages towards a pro-inflammatory phenotype preserving their pro-invasive and pro-angiogenic capacities. Sci Rep 6:1–15; 2016.

Prendergast GC, Jaffee EM. Cancer Immunotherapy: Immune Suppression and Tumor Growth, Second Edition. Academic Press. 2013.

Reeves G. Chapter 14: Effects on Personnel. In: EM-1: Capabilities of Nuclear Weapons. DTRA-EM-1-CH-14 (R1), Defense Threat Reduction Agency, Fort Belvoir, VA; 2018.

Reynolds A, Rubin J, Clermont G, Day J, Vodovotz Y, Bard Ermentrout G. A reduced mathematical model of the acute inflammatory response: I. Derivation of model and analysis of anti-inflammation. J Theor Biol 242:220–236; 2006.

Romagnani S. Th1/Th2 cells. Inflamm Bowel Dis 5:285–294; 1999.

Sanghvi AS. Sunburn: Symptoms, Risk Factors, and Treatment Options. 2020.

Schultz GS, Chin GA, Moldawer L, Diegelmann RF. Principles of Wound Healing. In: Fitridge R and Thompson MM, eds. Mechanisms of Vascular Disease: A Reference Book for Vascular Specialists. University of Adelaide Press; 2011:423–449.

Segal RA, Diegelmann RF, Ward KR, Reynolds A. A differential equation model of collagen accumulation in a healing wound. Bull Math Biol 74:2165–2182; 2012.

Smirnova OA. Comparative analysis of the dynamics of thrombocytopoietic, granulocytopoietic, and erythropoietic systems in irradiated humans: A modeling approach. Health Phys 103:787–801; 2012.

Strudwick XL, Cowin AJ. The role of the inflammatory response in burn injury. In: Hot Topics in Burn Injuries. InTech; 2018.

Tiwari VK. Burn wound: How it differs from other wounds? Indian J Plast Surg 45:364–373; 2012.

Torres M, Wang J, Yannie PJ, Ghosh S, Segal RA, Reynolds AM. Identifying important parameters in the inflammatory process with a mathematical model of immune cell influx and macrophage polarization. PLoS Comput Biol 15:e1007172; 2019.

Valvis SM, Waithman J, Wood FM, Fear MW, Fear VS. The immune response to skin trauma is dependent on the etiology of injury in a mouse model of burn and excision. J Invest Dermatol 135:2119–2128; 2015.

Van Linthout S, Miteva K, Tschöpe C. Crosstalk between fibroblasts and inflammatory cells. Cardiovasc Res 102:258–269; 2014.

Wang C. Assessment and Physiology of Burns. In: Anesthesia for Trauma: New Evidence and New Challenges. Springer, New York, NY; 2014:271–289.

Wilkinson HN, Hardman MJ. Wound healing: Cellular mechanisms and pathological outcomes. Open Biol 10:200223; 2020.

Yáñez A, Coetzee SG, Olsson A, Muench DE, Berman BP, Hazelett DJ, Salomonis N, Grimes HL,

Goodridge HS. Granulocyte-monocyte progenitors and monocyte-dendritic cell progenitors independently produce functionally distinct monocytes. Immunity 47:890–902; 2017.

Yang Q, Berthiaume F, Androulakis IP. A quantitative model of thermal injury-induced acute inflammation. Math Biosci 229:135–148; 2011.

MATLAB 2020b. The MathWorks, Inc., Natick, MA, U.S.A.; 2020.

# Section 10. Abbreviations, Acronyms and Symbols

| Acronym | Meaning |
|---|---|
| DTRA | Defense Threat Reduction Agency |
| GSA | Global Sensitivity Analysis |
| HSCs | Hematopoietic Stem Cells |
| HENRE | Health Effects from Nuclear and Radiological Environments |
| NUDET | Nuclear Detonation |
| ODE | Ordinary Differential Equation |
| TDPM | Time-Dependent Physiological Model |
| TR | Technical Report |